Finite-amplitude instability in growth step trains with overlapping step supply fields

Franz Rosenberger, Hong Lin, and Peter G. Vekilov*
Center for Microgravity and Materials Research, University of Alabama in Huntsville, Huntsville, Alabama 35899
(Received 3 June 1998; revised manuscript received 25 September 1998)

We have expanded our numerical model of coupled bulk transport in solution and interfacial kinetics in crystal growth [Vekilov, Lin, and Rosenberger, Phys. Rev. E **55**, 3202 (1997)] by explicitly including adsorption on and desorption from terraces between growth steps, surface diffusion, and incorporation into steps. At the steps, the surface (adsorption layer) concentration C_s is assumed to be either continuous, i.e., have the same values at the top and bottom of a step, or to be discontinuous, i.e., to take on different, respective terrace-width-dependent values. In order to maximize spatial resolution about individual steps, we use a mesoscale grid at the solution-crystal interface, which moves with the step positions and adjusts to the changing terrace widths during the simulation. This model was evaluated with transport and kinetics parameters characteristic for the growth of lysozyme crystals from aqueous solutions. With continuous C_s at steps, the simulations reproduced the results of our previous model in which the step supply field overlap was only indirectly accounted for by a step-density-dependent deceleration parameter in the step velocity. When discontinuities in C_s were allowed, significantly higher bunching instability resulted. More importantly, we found that step bunching may or may not occur, depending on the specific step-density perturbation (magnitude, sign and rate of step-density change). This is why linear stability analyses do not predict the unsteady growth behavior observed in our experiments and obtained in our simulations. [S1063-651X(99)03203-1]

PACS number(s): 81.10.Aj, 05.70.Ln, 61.72.Cc, 68.35.Ct

I. INTRODUCTION

Recently, employing a high-resolution laser interferometry technique with digital image and signal processing [1], we discovered kinetic instabilities in layer spreading during the crystallization of the protein lysozyme from solution [2]. We found that, even under steady solution conditions, the locally measured normal growth rate and growth step (layer edge) density fluctuate by up to several times their average values. The mechanism underlying these fluctuations was deduced from investigations of the dependences of the fluctuation amplitudes and frequencies on the type of layer source, average crystal growth rate, and crystal size (i.e., bulk transport length scale [3]) during growth from unstirred solutions. We concluded that the kinetics unsteadiness represents the response of the coupled bulk-transport/interfacial-kinetics processes to the intrinsic stochastics of layer generation [2,4]. This response is similar to stability loss under constant external conditions that occurs in a variety of systems operating far from equilibrium under mixed control conditions; for an in-depth review see Ref. [5]. Further support of the inferred mechanism of fluctuation generation stems from experiments in which the role of bulk transport in the overall growth rate control of lysozyme crystals was reduced by forced solution flow [6,7]. As expected from the model, this shift in working point towards kinetics control resulted in significant reduction of the fluctuation amplitudes. Thus, beyond their practical significance, that stems from the associated striae formation and expected reduction in the utility of the grown crystals [2,8], these phenomena merit detailed studies as a model for kinetic instability and spatiotemporal pattern formation in the form of nonlinear waves [5] in an open flow, albeit nonhydrodynamic system [9].

To gain further insight, we designed a numerical model of the coupled bulk transport and nonlinear interfacial kinetics processes in protein crystallization [10]. On evaluation with experimentally determined kinetic coefficients for bulk transport [11] and interfacial processes of lysozyme [12], this model quantitatively reproduced the experimentally observed kinetics unsteadiness. Changes of the governing parameters toward stronger kinetics control and higher nonlinearity in kinetics, respectively, decreased and increased the fluctuation amplitudes, as anticipated from the above instability considerations. We also found that discrete perturbations develop into an increasingly steeper step bunch *and* multiply through a cascade of new bunches that form ahead of the first one. This growth and spreading of the triggering perturbation occurs through deformation of the interfacial solute supply field of the growth steps.

Interestingly, the instability wavelengths and frequencies observed in our experiments and simulations [2,10] are quite different from those predicted by linear stability analysis of step motion in flowing and stagnant solutions [13–16]. Even on inclusion of the mutual retardation of steps due to their supply field overlap, these analyses predict stability of equidistant step trains under conditions that result in instabilities in our system [17]. Hence, the aim of this paper is to numerically study the stability/instability transition of a system representative of lysozyme growth by following the evolution of step bunches triggered by perturbations of different amplitudes. Such transitions may involve a nonlinearly amplified response to small-scale perturbations. Since sequences of kinetic processes are particularly prone to respond nonlinearly, we have included in our model all currently known stages of the growth mechanism. For this, we have expanded our model of coupled bulk transport and interfacial kinetic [10]

*Author to whom correspondence should be addressed. Electronic address: peter@cmmr.uah.edu

to explicitly include solute adsorption at the terraces between steps and diffusion along the surface followed by either desorption, or incorporation into steps. We ignore direct incorporation from the solution into steps, since we have shown earlier that, if present in our system, it contributes only insignificantly to the interstep interactions [2].

In the following, we provide the set of governing equations and boundary conditions comprising our model in Sec. II. In Sec. III, the numerical approach taken in Ref. [10] is refined by introducing at the solution-crystal interface a mesoscale grid that moves with the growth step positions and adjusts to the changing step positions and terrace widths. Results obtained with partially measured and partially inferred kinetic parameters for lysozyme are presented and discussed in Sec. IV. The conclusions are presented in Sec. V.

II. MODEL

A. Diffusive bulk transport

The geometry of the diffusive bulk transport is based on the setup used in our experimental investigations [1,2] and is the same as in Ref. [10]. The model solution consists of the protein lysozyme in solvent (buffer and precipitant [1,2,18,19]). The initial lysozyme mass concentration in the solution is $C^0=50$ mg/ml. At 12 °C, and the precipitant concentration and buffer pH used in the experiments, the solubility of lysozyme is $C^{\mathrm{eq}}=3.1$ mg/ml [19]. Hence, the initial value of the supersaturation $\sigma^0=\ln(C^0/C^{\mathrm{eq}})$ is 2.78. Further details of the bulk transport model, including boundary conditions at the container walls, are provided in Ref. [10].

The volume-surface exchange process is governed by the interfacial boundary condition

$$D\left.\frac{\partial C}{\partial z}\right|_{\mathrm{intf}}=\left(\frac{D}{\Lambda}\right)C\Big|_{\mathrm{intf}}-\frac{C_s}{\tau}, \tag{1}$$

where $D/\Lambda=\beta_{\mathrm{ad}}$ is the kinetic constant for adsorption of solute from the solution at the interface into the adsorbed layer with D the bulk diffusivity and Λ a characteristic length proportional to the resistance for adsorption, C_s is the surface (adsorption layer) solute concentration, and τ is the mean lifetime of an adsorbed molecule on the surface. Note that, in contrast to the earlier model where only steps formed sinks for the bulk transport, in the current model, as expressed by Eq. (1), all points on the interface present potential sinks.

B. Surface diffusion

At the supersaturation used in the simulations, lysozyme crystals grow by layer generation and spreading [12]. Adsorbed solute molecules diffuse on the terraces. The conservation equation for the adsorbed solute is

$$\frac{\partial C_s}{\partial t}=D_s\frac{\partial^2 C_s}{\partial x^2}+D\left.\frac{\partial C}{\partial z}\right|_{\mathrm{intf}}, \tag{2}$$

where the surface diffusivity D_s is assumed independent of the protein surface concentration. As in Eq. (1), the second term on the right-hand side of Eq. (2) represents the surface-volume exchange flux.

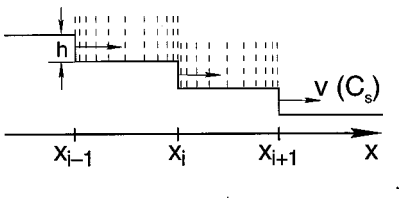

FIG. 1. Steps in the interface with one-dimensional surface diffusion grid and attached vertical grid lines of the mesoscale domain.

Following Refs. [20,21], we assume that the flux into a step, j_s, is proportional to the deviation of the surface concentration C_s at the step from its equilibrium value C_s^{eq}, i.e., to the linear supersaturation at the step. On the ith terrace, bound by the ith and $(i+1)$th steps (located at $x=x_i$ and x_{i+1}, respectively) these fluxes are

$$j_s(x_i+)=D_s\left.\frac{\partial C_s}{\partial x}\right|_{x_i+}=\beta_s(C_s(x_i+)-C_s^{\mathrm{eq}}), \tag{3a}$$

$$j_s(x_{i+1}-)=-D_s\left.\frac{\partial C_s}{\partial x}\right|_{x_{i+1}-}=\beta_s(C_s(x_{i+1}-)-C_s^{\mathrm{eq}}). \tag{3b}$$

Here, β_s is the kinetic coefficient for incorporation of adsorbed molecules into steps, and $-$ and $+$ denote, respectively, the terrace to the left and right of a step moving in the positive x direction, see Fig. 1.

The set of the bulk diffusion equation and Eqs. (1)–(3) represent the assumed pathway of solute from the solution into the crystal. It consists of bulk diffusion, followed by exchange of molecules between the adsorbed layer and the solution adjacent to the interface, diffusion of adsorbed molecules towards steps and incorporation into steps, which results in step motion.

Since jumps of adsorbed molecules over the steps require a higher activation energy than interterrace diffusion [22,23], similar to other recent works (e.g., Ref. [24]), in the majority of the cases presented here we treat each terrace as an independent surface concentration domain. Thus, we allow for

$$C_s(x_i-)\neq C_s(x_i+). \tag{4}$$

However, since in some cases such diffusion across the steps is possible [25], we also explore the consequences of the condition

$$C_s(x_i-)=C_s(x_i+). \tag{5}$$

In all cases, we assume equal kinetic coefficients for incorporation from the left terrace β_s^- and the right terrace β_s^+ and express them in the form

$$\beta_s^-=\beta_s^+=\beta_s=0.5D_s/\Lambda_s. \tag{6}$$

Here Λ_s is a characteristic length proportional to the resistance for incorporation from the surface into steps. Note that the restriction of Eq. (6) can be readily relaxed and the consequences of asymmetric kinetics of incorporation into steps [22] for step train stability can be studied without other changes in the model.

We will see in Sec. II D that the characteristic surface diffusion velocity D_s/λ_s is of the order of 5 μm/s. This is an order of magnitude higher than the typical step velocity for lysozyme crystal growth of 0.5 μm/s [12]. Hence, the neglect of an advective contribution, associated with step motion, in Eqs. (3) is well justified.

Furthermore, as in Refs. [20,21,26,27] we consider the steps to be sufficiently rough, i.e., to possess high kink density so that diffusion along their edges can be ignored. Thus, the restriction of our model to two dimensions, with the steps represented as point sinks for the adsorbed solute, is also well justified.

C. Step motion and step generation

The surface flux into a step determines its velocity according to

$$v = j_s \Omega/\hbar, \tag{7}$$

where $\Omega = 3\times10^{-20}\,\mathrm{cm}^3$ [28,29] is the volume per lysozyme molecule in the crystal and $h = 1.02\times10^{-6}\,\mathrm{cm}$ is the step height [30–32]. Thus, accounting for the fluxes into a step from the left and right, using Eqs. (4), the velocity of the ith step at x_i, can be expressed as

$$v_i = \frac{\Omega}{h}(j_s^- + j_s^+) = \frac{\Omega}{h} \times\{\beta_s[C_s(x_i-) - C_s^{\mathrm{eq}}] + \beta_s[C_s(x_i+) - C_s^{\mathrm{eq}}]\}. \tag{8}$$

Steps that have a higher velocity will eventually catch up with slower ones. We assume that, due to entropic repulsion between steps [33], a pair of steps cannot form a double step or an overhang. Somewhat arbitrarily, the repulsive potential is chosen as a ''hard-body'' interaction, with the characteristic distance between the steps set at five lattice parameters ($=5h$). The velocity of the trailing step in a pair that reached this critical separation is adjusted such that a closer approach is prevented.

Growth on a facet ceases when all initially imposed steps have reached the center and the facet has become singular. Hence, growth can only be sustained through the replenishment of growth steps. Therefore, in accordance with recent findings for lysozyme at the supersaturation used in the simulations [12], we assume that growth steps are generated by two-dimensional (2D) nucleation at the edge of the crystal, where the supersaturation is the highest [3,34,35].

The probability for the generation of a new growth step within a time t_{nucl} after a preceding two-dimensional nucleation event can be expressed as [36]

$$P(t_{\mathrm{nucl}}, C_s^{\mathrm{edge}}) = 1 - \exp(-I_0 t_{\mathrm{nucl}}), \tag{9}$$

where I_0 is the steady-state rate of 2D nucleation [37],

$$I_0 = A C_s^{\mathrm{edge}} \exp(-B/\sigma_s^{\mathrm{edge}}), \tag{10}$$

and

$$\sigma_s^{\mathrm{edge}} = \ln\left(\frac{C_s^{\mathrm{edge}}}{C_s^{\mathrm{eq}}}\right). \tag{11}$$

The constant A ($\mathrm{cm}^2/\mathrm{mg\,s}$) contains activation and surface energies as well as frequency factors [38,39], and $B = \pi\Omega\gamma^2 h/(k_B T)^2$, with $\gamma = 1\,\mathrm{erg/cm}^2$ [40,41] the step free energy, and k_B the Boltzmann constant. At 12 °C ($T = 285\,\mathrm{K}$), this results in $B = 67.2$. Note that in Eqs. (9)–(11) we use the surface supersaturation as nucleation driving force, rather than the interfacial bulk supersaturation employed in Ref. [10]. Since C_s^{edge} and, thus, σ_s^{edge} depend on the distance the prior step has traveled on the surface, this formulation accounts for the effect of the velocity of the prior step on the nucleation probability of the following step, i.e., the so-called back-stress effect [26,42].

All results presented in this paper were obtained based on a deterministic nucleation mode. A new layer is generated whenever $P > \varepsilon$. We set $\varepsilon = 0.99$. Unless stated otherwise, the value of the constant A is chosen such that at the initial surface supersaturation at the nucleation site $\sigma_s^{0,\mathrm{edge}}$ [see Eq. (12)], the slope of the resulting step train equals p^0. Thus, the nucleation time for the first time step should be equal to the ratio $h/R^0 = h/p^0 v(C_s^{0,\mathrm{edge}})$, which leads to

$$A = \frac{\ln(1-\varepsilon)}{C_s^{0,\mathrm{edge}} t_{\mathrm{nucl}} \exp(-B/\sigma_s^{0,\mathrm{edge}})} = \frac{p^0 v(C_s^{0,\mathrm{edge}}) \ln(1-\varepsilon)}{C_s^{0,\mathrm{edge}} h \exp(-B/\sigma_s^{0,\mathrm{edge}})}, \tag{12}$$

where $C_s^{0,\mathrm{edge}}$ and $\sigma_s^{0,\mathrm{edge}}$ are the initial values of these variables at the edge.

D. Determination of step kinetics parameters

For an equidistant step train at steady state, and assuming that bulk transport is significantly faster than the interfacial processes, our model is equivalent to that of Ref. [21]. Thus, we can extract the values of the kinetics constants for adsorption, desorption, surface diffusion and incorporation into steps from the surface by correlating our experimentally determined $v(\sigma)$ to the theoretically derived dependences in Ref. [21]. The experimental data are best described by [12] (see also discussion in Ref. [10])

$$v = \frac{b\sigma}{1+kp}, \tag{13}$$

with $b = 15\times10^{-5}\,\mathrm{cm/s}$ and $k = 500$. From independent experiments, we also know the value of the characteristic surface diffusion length, $\lambda_s = 2\times10^{-4}\,\mathrm{cm}$ [43]. As shown in Ref. [43], in the case of rapid bulk transport, in terms of Ref. [21],

$$b = \frac{\lambda_s^2 D\Omega C}{\Lambda\Lambda_s h} \quad \text{and} \quad k = \frac{\lambda_s^2}{\Lambda_s h}. \tag{14}$$

Equations (14) allow us to determine the values of Λ and Λ_s. To find the characteristic adsorption time τ, we use the relation

$$\lambda_s^2 = D_s \tau. \tag{15}$$

TABLE I. Parameters and initial conditions used in the simulations of the ''base case.'' For sources and derivations see text.

Parameters	Notation	Value	Unit
Bulk diffusivity	D	1.06×10^{-6}	cm^2/s
Adsorption resistance	Λ	0.22	cm
Surface diffusivity	D_s	1.0×10^{-7}	cm^2/s
Characteristic surface diffusion length	λ_s	2.0×10^{-4}	cm
Characteristic incorporation resistance	Λ_s	7.8×10^{-5}	cm
Mean lifetime of adsorbed molecules	τ	0.4	s
Temperature	T	285	K
Initial vicinal slope	p^0	5.0×10^{-3}	
Initial bulk protein concentration	C^0	50	mg/ml
Equilibrium bulk protein concentration	C^{eq}	3.1	mg/ml
Initial surface protein concentration	C_s^0	9.1×10^{-5}	mg/cm^2
Equilibrium surface protein concentration	C_s^{eq}	5.6×10^{-6}	mg/cm^2

There have been no determinations of D_s for lysozyme. However, for the protein canavalin, $2\times10^{-8}<D_s<7\times10^{-7}\,cm^2/s$ [44]. Hence, we assume $D_s=1\times10^{-7}\,cm^2/s$, which is about an order of magnitude lower than the bulk diffusivity, $D=1.06\times10^{-6}\,cm^2/s$ [11].

Before growth has started, or after equilibrium is reached, $\partial C/\partial z=0$ throughout the solution including $z=0$. Hence, from Eq. (1),

$$C_s^0=\frac{D\tau}{\Lambda}C^0 \quad \text{and} \quad C_s^{eq}=\frac{D\tau}{\Lambda}C^{eq}. \tag{16}$$

From these relations, we determine the initial and equilibrium values of C_s.

The values of the parameters and initial conditions used in the simulations of the growth behavior of the protein lysozyme are summarized in Table I, with the initial slope $p^0=5\times10^{-3}$ representing an average value found in numerous experiments [12,43].

III. NUMERICAL APPROACH

The ''global'' computational grid used for the diffusive bulk transport is identical to that used in Ref. [10]. As in that earlier work, the concentration distribution at the interface was obtained in a mesoscale grid that covers the narrow interfacial area. The horizontal grid spacing in the mesoscale domain is based on a nonuniform one-dimensional surface grid used for the C_s computations. This 1D grid is moved with the steps and is adjusted according to the changing widths of the terraces at each time step in the following way. When the two steps that bound a terrace are located at the positions x_i and x_{i+1}, nine additional grid points $x_{i,j}^g$ are distributed over this ith terrace according to

$$x_{i,j}^g=\left(\frac{x_{i+1}-x_i}{2}\right)\left[\cos\left(\frac{2j+1}{2(k-1)}\pi\right)+1\right], \quad j=1,...,k-2. \tag{17}$$

Hence, there are $k=11$ grid points per terrace, and with typically 150 steps/terraces on the interface, the surface diffusion mesh contains approximately 1500 grid points. Note that the distribution given by Eq. (17), which represents the zeroth nodes of the Chebyshev polynomials, results in finer grid spacing close to the terrace edges, the steps. This mesh nonuniformity, together with the step-bound motion of the grid, ensures high accuracy of the calculation of the surface flux into the steps. The vertical grid lines in the mesoscale domain, which extend to the first horizontal grid line above the interface in the global grid, i.e., to $z=25\,\mu m$, move with the expanding/contracting mesh of the 1D surface domain. Since, due to annihilation at the center of the facet (see below) and generation at the edge, the number of steps on the interface changes continuously, as does the exact number of grid points in the 1D surface domain and, thus, in the mesoscale domain.

In the z-direction, the m-s domain contains nine horizontal grid lines between its top boundary and the crystal surface; see Fig. 1(b). These grid lines are generated according to the power law

$$z_i^g=z_1^g+\left(\frac{i-1}{k-1}\right)^a(z_k^g-z_1^g), \quad i=1,...,k. \tag{18}$$

Here $k=11$, as in the surface diffusion grid, with $z_1^g=0$, and $z_k^g=25\,\mu m$. The nonuniformity parameter a was set at 2.05 so that $z_2^g-z_1^g=0.22\,\mu m$, which corresponds to the average mesh size in the x direction. Note that we used here 11 horizontal grid lines to cover the mesoscale domain, compared to 21 in Ref. [10]. Detailed tests showed that this reduced mesh still results in sufficient accuracy and reproducibility. Equation (18) is also used to calculate the positions of the *vertical* grid lines in the mesoscale domain to the left of the left crystal edge by substituting z for x.

As in our earlier model [10], the actual changes in interface position and shape were ignored in the transport simulations; see Refs. [10,35] for justification.

Step propagation was simulated as follows. When a new step is generated, the old steps are renumbered by substituting $i+1$ for i. When a step reaches the facet center, it is annihilated. The step positions x_i are moved along the continuous coordinate axis x at discrete time intervals Δt according to

$$x_i^{n+1}=x_i^n+v^n\Delta t, \tag{19}$$

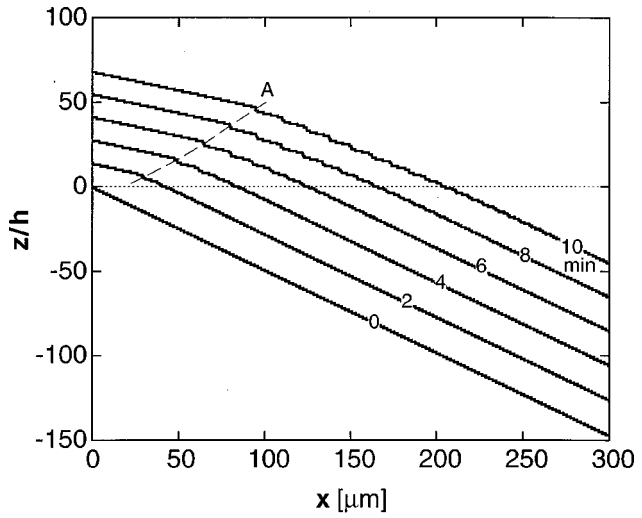

FIG. 2. Interface profiles obtained at various simulation times for the base case (the set of parameters in Table I, with $A=1.24\times10^{14}\,\mathrm{cm^2/mg\,s}$) and assuming discontinuous C_s across steps; i.e., no exchange of adsorbed solute between terraces. z values are in units of step height $h=102$ Å. Changes in z values at $x=0$ account for layers generated between the times noted, i.e., individual steps remain at their z while propagating to the right. The dotted horizontal at $z/h=0$ separates new and old steps. Dashed line, A traces the location of the initial step density perturbation.

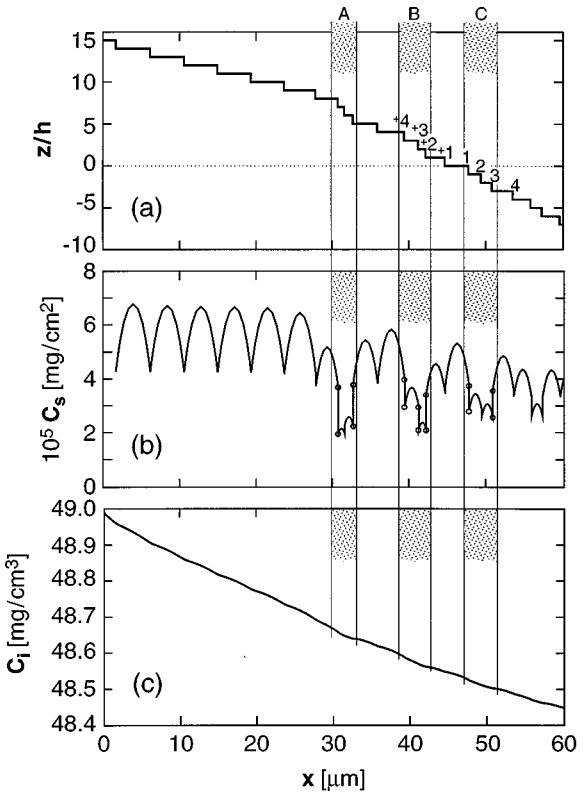

FIG. 3. Details of interfacial conditions after 2 min of growth. (a) Interface profile, 1 through 4 denote steps that were the closest to the edge at $t=0$; $+1$ through $+4$ denote first four newly nucleated steps. (b) Distribution of surface concentration C_s; note the sharp minima at steps. (c) Corresponding distribution of bulk concentration at the interface, $C_i=C|_{z=0}$.

where n and $n+1$ denote the successive time steps. The local values of the vicinal slope p_i are calculated as

$$p_i=\frac{h}{x_{i+1}-x_i}. \tag{20}$$

The local normal growth rate R is obtained from

$$R_i=p_i v_i. \tag{21}$$

Since the kinetic parameters for nucleation and growth are compatible with those used in Ref. [10], we expect similar values of step velocities, nucleation frequencies, and growth rates. Hence, we used the same simulation time step $\Delta t=0.025$ s.

The simulation procedure is very similar to the one used in Ref. [10].

IV. RESULTS AND DISCUSSION

A. Response to a large reduction in step production rate (base case)

First, we have investigated the evolution of the interface morphology using the basic set of parameters listed in Table I, allowing for discontinuity in C_s at the steps, as in Eq. (4). With $C_s^{0,\mathrm{edge}}=C_s^0$, Eq. (12) yields for this ''base case'' the preexponential factor in the nucleation rate, $A=1.24\times10^{14}\,\mathrm{cm^2/mg\,s}$. Simulations were carried out for a growth time of 60 min. Figure 2 illustrates the evolution of the interface profile for the first 10 min of this base case. The newly created step train has about half the step density of the initial train given by $p^0=5\times10^{-3}$. This is due to solute depletion in the solution adjacent to the interface and the corresponding decrease in the surface concentration. In accordance with Eqs. (9)–(11), a reduction in C_s^{edge} results in a decreased step generation (nucleation) rate and, hence, a reduced vicinal slope of the new step train.

Furthermore, Fig. 2 shows that this large perturbation in step spacing triggers a cascade of step bunches on the vicinal face. In this presentation, in which individual steps remain at constant z/h, one sees that steps move through bunches on their way to the facet center; that is, bunches move with a velocity v_{bunch}, which is distinctly lower than the average step velocity $\overline{v}$. This behavior is similar to that obtained in our earlier model [10] and related to predictions of the kinematic wave theory [45]. In that work, we accounted for interactions between growth steps only through a phenomenological parameter k without consideration of the details of surface diffusion [10].

Our current more detailed model allows us to elucidate the mechanism underlying this bunching and cascading process through interactions between the individual steps. For this, in Fig. 3 we show the profile of the interface segment at $t=2$ min together with the corresponding distributions of surface concentration C_s and interfacial solution concentration $C_i=C_{z=0}$. To emphasize the consequences of allowing for C_s discontinuity across steps, we have emphasized the concentration differences between the upper and lower side of select steps by data points for the respective bounding C_s values, see the small circles in Fig. 3(b). This $C_s(x)$ has local

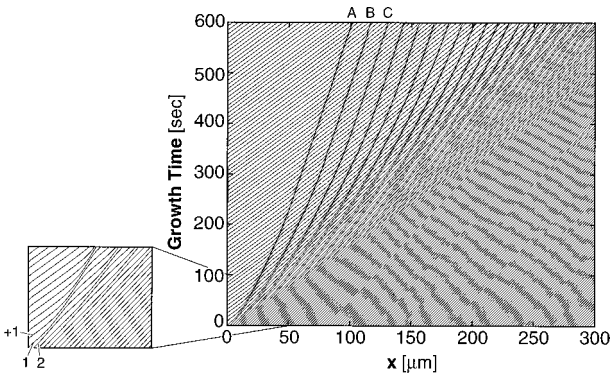

FIG. 4. Time dependence of positions of all steps during first 10 min of growth. Step bunches $A-C$ are the same is in Fig. 3. A 2:1 blowup of area ($x \leqslant 50\ \mu$m, $t \leqslant 100$ s) is shown.

minima at the locations of the steps which are sinks for the adsorbed solute, in agreement with analytical solutions obtained for the growth mechanism involving surface diffusion [21,26,27]. Note that the magnitude of strongly depends on the width of the terrace between two steps. As the distance between two steps decreases, C_s drops since the probability that adsorbed solute reaches either of the bounding steps during the mean lifetime τ is inverse proportional to the square of the terrace width. Since the C_i distribution is coupled to $C_s(x)$, its local minima at steps in bunches are deeper than at wider separated steps, see Fig. 3(c).

The $C_s(x)$ distributions also shed light on the mechanism of step motion through bunches and the associated cascading process. For instance, Fig. 3(b) shows that at that moment step 1 is much better supplied from its upper terrace than step 2 and, thus will push deeper into bunch *C*. In parallel, step 3 is better supplied from its lower terrace and, therefore, will pull away from the bunch. This, in turn, will widen the terrace between steps 3 and 2, thus increasing the solute supply to step 2 from its lower terrace. As a consequence, step 2 will eventually be able to also pull away from bunch *C*, etc.

The spreading of the bunching cascade over the whole facet can be readily followed in the long-term traces of the step positions presented in Fig. 4. Overall, we see that the initial perturbation, that stems from the acceleration of step one due to the delayed nucleation of step $+1$ (see above), develops into a step bunch *A* and induces a cascade of step bunches *B*, *C*,.... By tracing the origins of these new step bunches, one can see that the cascading wave propagates with a relatively constant velocity and reaches $\sim 280\ \mu$m at $t = 600$ s. In addition, while the step bunches propagate towards the facet center and individual steps continuously move through them, the bunches tend to steepen.

More detailed insight into the changes in number and, in particular, in steepness of the step bunches is provided by the time traces of the vicinal slope *p*, recorded at three locations on the half-facet, that are presented in Figs. 5(a)–5(c). Close to the edge at which growth steps are generated [Fig. 5(a)] only the initial macrostep passes at ~ 1 min through the sampling point. The consecutive reduced slope characterizes the newly generated step train seen in Fig. 2. At the middle and right locations, a forerunner (barely discernible change in step spacing) is followed by a cascade of macrosteps which grow in number on their way to the facet center. At both locations, the last bunch to arrive is the initial macrostep, i.e., bunch *A* in Figs. 2–4. The number of step bunches created in front of bunch *A* and registered at the right location [Fig. 5(c)] are about twice the number registered at the middle [Fig. 5(b)]. This is to be expected given a rather constant

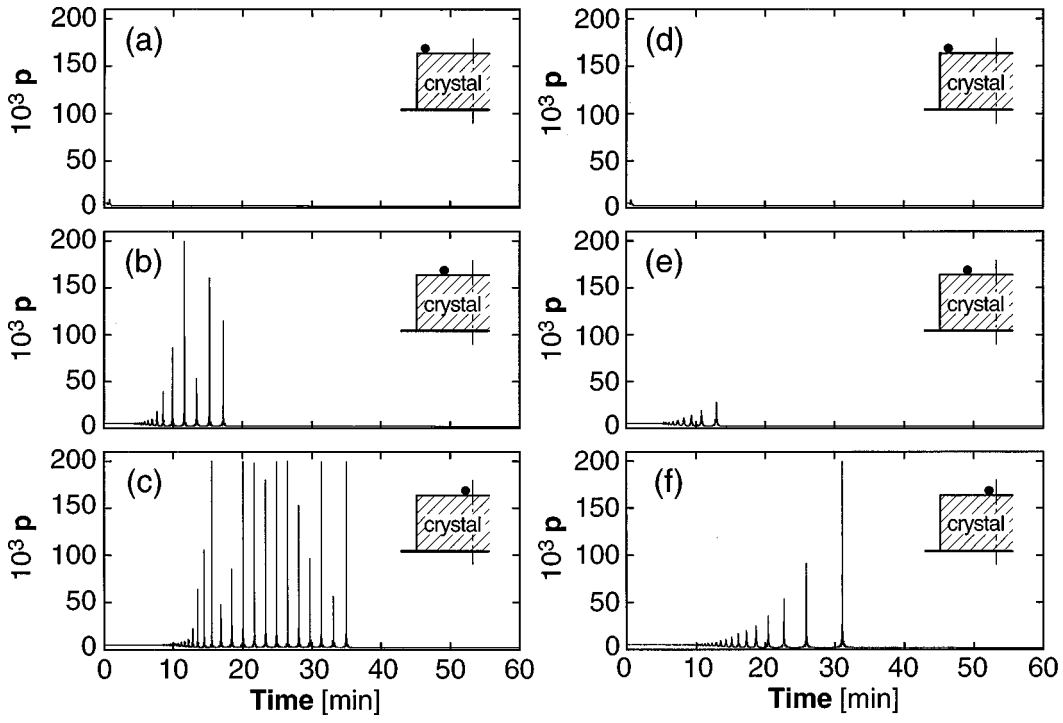

FIG. 5. Time traces of slope *p* at three interface locations, 15, 150, and 285 μm from the crystal edge, obtained for base case and: (a)–(c) discontinuous C_s at steps, same as for Figs. 2–4; (d)–(f) continuous C_s at steps.

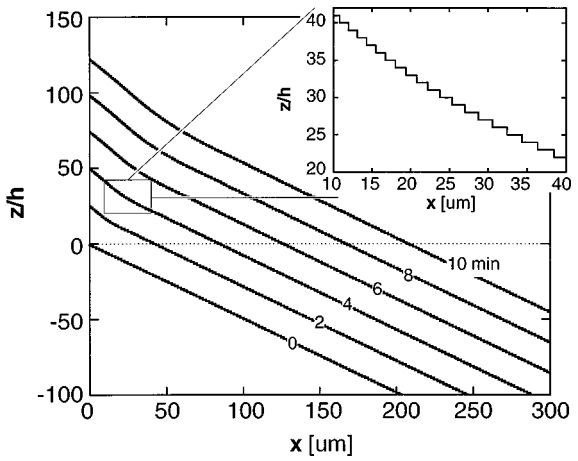

FIG. 6. Interface profile response to increase in step production rate ($A=8.16\times10^{17}$ cm^2/mg s). No bunching occurs; vicinal face is morphologically stable.

cascading wave velocity and twice the distance over which step bunches can evolve.

The above step pattern evolution is similar to the one obtained with simpler model assumptions in Ref. [10]. However, the number of step bunches, their frequency, and the maximum slope reached in a step bunch are considerably higher in the present case. This means that the instability in response to individual step density perturbations, as well as in the creation of new step bunches through the cascading mechanism is higher. As suggested by the increased step-train instability obtained in various theoretical analyses that assume asymmetric step kinetic coefficient β_s [46–48], the above strong response might be due to the discontinuity of C_s at the steps allowed for in this refined model. To test this, a base case was run with imposed C_s continuity, see Eq. (5). The resulting $p(t)$ traces at the three locations on the half-facet are presented in Fig. 5(d)–5(f). We see that this restriction causes an increase in step train stability: the number of step bunches, the bunching frequency, and the slope in the bunches are significantly reduced. The reason is that this constraint effectively averages C_s at a step, say step 2 at $t=25$ s in Fig. 3. The resulting increase in velocity of this step increases the time needed for step 3 to escape the proximity of step 2 to initiate a new bunch.

All following simulations were performed allowing for discontinuous C_s at the steps, Eq. (4).

B. Response to a large increase in step density

For the base case, we have recognized an increase in terrace width between the trailing old step 1 and the first new step $+1$ to instigate step bunching. Similarly, one might expect a narrower new terrace to trigger an instability in the original, equidistant step train. Hence, we have performed a simulation with a large increase in new step density. This was achieved by setting the preexponential coefficient in Eq. (12) to $A=8.16\times10^{17}$ cm^2/mg s from the 1.24×10^{14} cm^2/mg s used in the base case.

The results of this run are presented in a series of interface profiles in Fig. 6. No step bunches resulted in this case. One sees that the new steps rapidly adjust their spacing to essentially that of the initial step train (see also the inset in Fig. 6). This strongly suggests that the step bunching and cascading observed for this system in response to different perturbations present a finite amplitude instability, in contrast to the instabilities predicted earlier by linear stability analyses [14–16].

The step dynamics that underlie this step train stability become clear by a closer inspection of the patterns resulting from this perturbation. The closer spacing between steps 1 and $+1$ delays step 1 (for the notations, see above). This accelerates step 2 that zooms forward to catch up with step 3 and cause a bunch. The situation appears identical to that illustrated in the blown up area in Fig. 4, with the only difference being the number of the accelerated step: 2 instead of 1. However, this secondary nature the acceleration is crucial for its consequences: the step acceleration is weaker and the velocity of step 2 adjusts to that of step 3 without causing a bunch. The sensitivity of the step patterns to the magnitude of the step acceleration is in the roots of the stability of the step train with respect to small perturbations.

C. Dependence of response on rate of step-density change

To further explore this finite amplitude instability, we have performed simulations in which the rates, i.e., the magnitude of the growth step-density changes imposed per simulation time step was varied. In the first of these runs, we decreased A linearly over the first 10 min from 1.7×10^{16} cm^2/mg s to the 1.24×10^{14} cm^2/mg s of the base case. (The value of 1.7×10^{16} was determined in exploratory runs to yield essentially the same new step spacing as that given by the initial vicinal slope p^0.) This linear change in A results in an exponential increase in step nucleation time [see Eqs. (9) and (10)] and, similarly, in new terrace width.

Figure 7(a) presents the results, with the inset illustrating the time trace of the nucleation time. One sees that the initial low rate of step density (nucleation time) change does not result in bunching. A cascade of macrosteps forms only in response to the steep change that sets in at approximately 10 min. The importance of the perturbation magnitude is further underscored by comparing Fig. 2 to the 8- and 10-min profiles in Fig. 7(a). Although in the latter two profiles a step-density perturbation associated with *lower* slope of the newly generated step is present, no step bunching or cascading ensues. Bunches form only after this slope difference becomes substantial in the 12- and 14-min profiles. This well corroborates our contention that the above step bunching cascades form only in response to step-density perturbations of sufficient amplitude.

Note that the different response to small and large density perturbation should not be caused by different distribution of their Fourier modes. The slope changes discussed here are represented by the Heaviside step function. Thus, the corresponding Fourier spectra have identical frequency distributions, with the amplitudes proportional to the ratio of the initial to final slope values, i.e., to the perturbation magnitudes.

This insight is further rounded out by the results of a simulation in which A was set to 8.16×10^{17} cm^2/mg s during the first 10 min and then abruptly decreased to 1.7×10^{16} cm^2/mg s. Independent runs have shown that neither of these values, when individually applied to the base case,

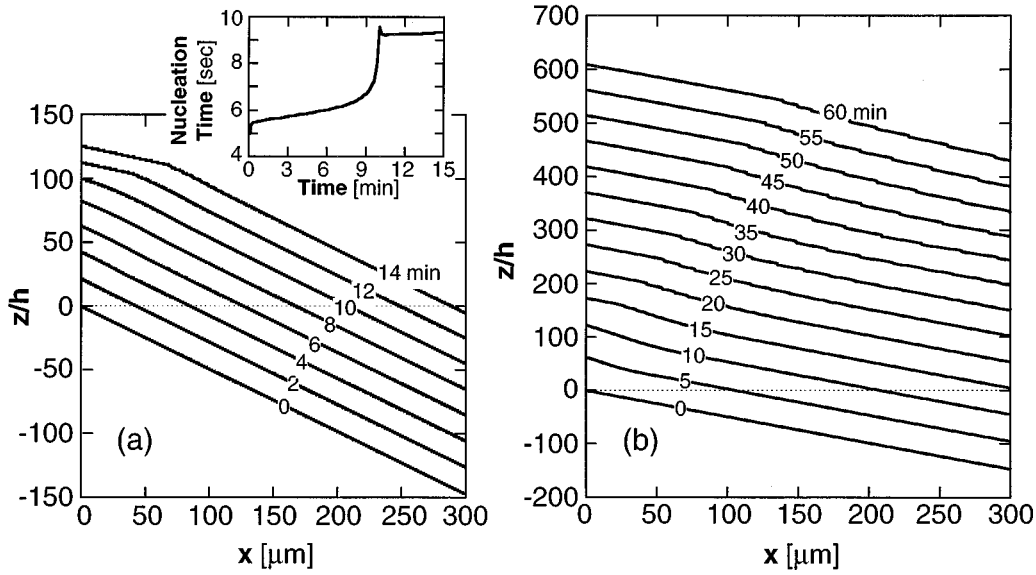

FIG. 7. Interface profiles response to (a) varying rate of decrease in step production rate (linear decrease of A from 1.7×10^{16} to 1.24×10^{14} cm^2/mg s during first 10 min). Inset: corresponding nucleation time trace. Note that although a step density perturbation (*lower* slope) is present already at 8 and 10 min, bunching and cascading sets in only at 12 min, when the rate of change becomes high. (b) Abrupt decrease of A from 8.16×10^{17} to 1.7×10^{16} cm^2/mg s at $t=10$ min.

result in bunching. However, bunching should occur in response to the sudden change from the steeper vicinal slope resulting from the first value, to the much lower one resulting from the second one. This is confirmed by the results in Fig. 7(b). First we see an increase in vicinal slope, as in the case of Fig. 6, followed by a bunching cascade in response to the lower A, which, when applied to the p^0 of the base case, caused nothing. Note also that these results refute a hypothetical instability scenario (linear or nonlinear), with the vicinal slope as the control parameter.

D. Comparison with linear stability theories

For a head-on comparison with linear stability theories [13–16], we set the preexponential coefficient in the nucleation rate equation, Eq. (10), to 1.7×10^{16} cm^2/mg s. This value ensures approximate preservation of the initial slope/step density on the crystal face even with decreasing supersaturation at the location of step generation. If a simulation is run with this value, no step bunching is observed in spite of the slight misfit between the initial and the newly developing slope. For the intended tests, after 5 min of growth via an equidistant step train, we imposed a 5% harmonic perturbation on step density by shifting each step by $\tilde{x}_i = 0.05(x_i - x_{i-1})\sin(2\pi x_i/\hat{x})$, where x_i and x_{i-1} are the positions of ith and $(i-1)$th steps at 5 min, and $\hat{x}$ is the perturbation wavelength. We chose three values of $\hat{x}$: 50, 100, and 200 μm, that cover the range of step bunching wavelengths observed in the experiments and simulations [2,4,10].

The results of these runs were output in terms of series of interfacial profiles and step density traces at three face locations, similar to Figs. 2 and 5, respectively. Both groups of results showed no step bunching for simulated growth times as long as 1 h. This is not surprising: if a Heaviside step-function perturbation, which is equivalent to a series of harmonic perturbations of various frequencies and amplitudes, does not cause step bunching, it is unlikely that a single harmonic perturbation may do so.

Based on these results, we suggest that the macrostep formation associated with the growth kinetics fluctuations observed in our experiments with the protein lysozyme [2] are triggered by major step-density variations. Such variations may arise from the intrinsically stochastic nature of two-dimensional nucleation. In the case of step generation by dislocations, they may be the result of the interaction between steps originating at several dislocations in a complex dislocation source, or by obstacles in the steps' pathway [49]. This conclusion is supported by numerous observations of differences in fluctuation amplitudes and time scales on crystals with different growth step sources [2,4], as well as by the recorded variations in unsteady behavior following changes in step source activity on the same crystal [4,50].

VI. SUMMARY AND CONCLUSIONS

We have explicitly included adsorption and diffusion on, and desorption from, growth terraces, together with incorporation into steps in a numerical model of coupled bulk transport and interfacial kinetics in crystal growth. The model was evaluated with parameters characteristic of the crystallization of the protein lysozyme. The results show that discontinuity in the surface concentration at steps, which can arise from higher surface diffusion activation barriers at the steps, leads to significantly higher bunching instability. When continuous surface concentration was assumed, the simulations reproduced the results of a simplified model in which step supply field overlap was accounted for by introducing a de-

celeration factor proportional to step density in the step-velocity/supersaturation dependence [9].

More importantly, the simulations show that a step-density perturbation, depending on its amplitude, sign, and rate of step-density change, may or may not evolve into a step bunching cascade. This explains why linear stability approaches, in which the evolution of the response is independent of the perturbation amplitude, do not yield the unsteady growth kinetics obtained in our experiments and simulations.

ACKNOWLEDGMENTS

We thank A. A. Chernov and S. Coriell for stimulating discussions. L. Carver expertly prepared the figures. Support by the Microgravity Science and Applications Division of NASA, by the State of Alabama through the Center for Microgravity and Materials Research at the University of Alabama in Huntsville, and by NATO is gratefully acknowledged.

[1] P. G. Vekilov, L. A. Monaco, and F. Rosenberger, J. Cryst. Growth **148**, 289 (1995).
[2] P. G. Vekilov, J. I. D. Alexander, and F. Rosenberger, Phys. Rev. E **54**, 6650 (1996).
[3] W. R. Wilcox, J. Cryst. Growth **37**, 229 (1977); **38**, 73 (1977); **65**, 133 (1983); H. D. Yoo, W. R. Wilcox, R. B. Lal, and J. D. Trolinger, *ibid.* **92**, 101 (1988).
[4] P. G. Vekilov, B. R. Thomas, and F. Rosenberger, J. Phys. Chem. **102**, 5208 (1998).
[5] M. C. Cross and P. C. Hohenberg, Rev. Mod. Phys. **65**, 851 (1993).
[6] P. G. Vekilov and F. Rosenberger, J. Cryst. Growth **186**, 251 (1998).
[7] P. G. Vekilov and F. Rosenberger, Phys. Rev. Lett. **80**, 2656 (1998).
[8] P. G. Vekilov and F. Rosenberger, Phys. Rev. E **57**, 6979 (1998).
[9] P. Huerre and P. Monkewitz, Annu. Rev. Fluid Mech. **22**, 473 (1990).
[10] P. G. Vekilov, H. Lin, and F. Rosenberger, Phys. Rev. E **55**, 3202 (1997).
[11] S. B. Dubin, G. Feher, and G. B. Benedek, Biochemistry **12**, 714 (1973); V. Mikol, E. Hirsch, and R. Giege, J. Biol. Chem. **213**, 187 (1990); M. Muschol and F. Rosenberger, J. Chem. Phys. **103**, 10 424 (1995).
[12] P. G. Vekilov and F. Rosenberger, J. Cryst. Growth **158**, 540 (1996).
[13] A. A. Chernov and T. Nishinaga, in *Morphology of Crystals*, edited by I. Sunagawa (Terra, Tokyo, 1987), p. 207.
[14] A. A. Chernov, Yu. G. Kuznetsov, I. L. Smol'skii, and V. N. Rozhanskii, Kristallografiya **31**, 1193 (1986) [Sov. Phys. Crystallogr. **31**, 705 (1986)]; A. A. Chernov, J. Cryst. Growth **118**, 333 (1992).
[15] A. A. Chernov, S. R. Corriel, and B. T. Murray, J. Cryst. Growth **132**, 405 (1993).
[16] S. R. Coriell, A. A. Chernov, B. T. Murray, and G. B. McFadden, J. Cryst. Growth **183**, 669 (1998).
[17] A. A. Chernov and S. R. Corriel (private communication).
[18] L. A. Monaco and F. Rosenberger, J. Cryst. Growth **129**, 465 (1993).
[19] F. Rosenberger, S. B. Howard, J. W. Sowers, and T. A. Nyce, J. Cryst. Growth **129**, 1 (1993).
[20] A. A. Chernov, Usp. Fiz. Nauk **73**, 277 (1961) [Sov. Phys. Usp. **4**, 116 (1961)]; *Modern Crystallography, Vol. III: Growth of Crystals* (Springer, Berlin, 1984), p. 123.
[21] G. H. Gilmer, R. Ghez, and N. Cabrera, J. Cryst. Growth **8**, 79 (1971).
[22] R. L. Schwoebel and E. J. Schipsey, J. Appl. Phys. **37**, 3682 (1966).
[23] D. W. Basset and P. R. Webber, Surf. Sci. **70**, 520 (1978).
[24] F. Lui and H. Metui, Phys. Rev. E **49**, 2601 (1994), and references therein.
[25] S. C. Wang and G. Ehrlich, Phys. Rev. Lett. **67**, 2509 (1991).
[26] J. P. van der Eerden, J. Cryst. Growth **56**, 174 (1982).
[27] W. K. Burton, N. Cabrera, and F. C. Frank, Philos. Trans. R. Soc. London, Ser. A **243**, 299 (1951).
[28] C. C. F. Blake, G. A. Mair, A. C. T. North, D. C. Phillips, and V. R. Sarma, Proc. R. Soc. London, Ser. B **167**, 365 (1967).
[29] L. K. Steinrauf, Acta Crystallogr. **12**, 77 (1959).
[30] S. D. Durbin and W. E. Carson, J. Cryst. Growth **122**, 71 (1992).
[31] S. D. Durbin, W. E. Carson, and M. T. Saros, J. Phys. D **26**, B128 (1993).
[32] J. H. Konnert, P. D'Antonio, and K. B. Ward, Acta Crystallogr., Sect. D: Biol. Crystallogr. **50**, 603 (1994).
[33] E. D. Williams and N. C. Bartelt, Science **251**, 393 (1991); N. C. Bartelt, T. L. Einstein, and E. D. Williams, Surf. Sci. Lett. **240**, L591 (1990).
[34] H. Lin, P. G. Vekilov, and F. Rosenberger, J. Cryst. Growth **158**, 552 (1996).
[35] H. Lin, F. Rosenberger, J. I. D. Alexander, and A. Nadarajah, J. Cryst. Growth **151**, 153 (1995).
[36] S. Toschev, A. Milchev, and S. Stoyanov, J. Cryst. Growth **13/14**, 123 (1972).
[37] A. J. Malkin, A. A. Chernov, and I. V. Alexeev, J. Cryst. Growth **97**, 765 (1989) and references therein.
[38] B. Mutafschiev, in *Handbook of Crystal Growth. I. Fundamentals Part A: Thermodynamics and Kinetics*, edited by D. T. J. Hurle (North-Holland, Amsterdam, 1993), p. 187.
[39] D. Kashchiev, in *Science and Technology of Crystal Growth*, edited by J. P. van der Eerden and O. S. L. Bruinsma (Kluwer, Dordrecht, 1995), p. 53.
[40] A. A. Chernov and H. Komatsu, in *Science and Technology of Crystal Growth*, edited by J. P. van der Eerden, O. S. L. Bruinsma (Kluwer Academic Publishers, Dordrecht, 1995), p. 329.
[41] P. G. Vekilov, L. A. Monaco, B. R. Thomas, V. Stojanoff, and F. Rosenberger, Acta Crystallogr., Sect. D: Biol. Crystallogr. **52**, 785 (1996).
[42] N. Cabrera and R. V. Coleman, in *The Art and Science of Growing Crystals*, edited by J. J. Gilman (Wiley, New York, 1963), p. 3.
[43] P. G. Vekilov, L. A. Monaco, and F. Rosenberger, J. Cryst. Growth **156**, 267 (1995).

[44] T. A. Land, J. J. De Yoreo, and J. D. Lee, Surf. Sci. **384**, 136 (1997).
[45] F. C. Frank, in *Growth and Perfection of Crystals*, edited by R. H. Doremus, B. W. Roberts, and D. Turnbul (Chapman and Hill, London, 1958), p. 411.
[46] G. S. Bales and A. Zangvill, Phys. Rev. B **41**, 5500 (1990).
[47] M. Uwaha, Phys. Rev. B **46**, 4364 (1992); J. Cryst. Growth **128**, 92 (1993).
[48] M. Sato and M. Uwaha, Phys. Rev. B **51**, 11 172 (1995).
[49] K. Maiwa, M. Plomp, W. J. P. van Enckevort, and P. Bennema, J. Cryst. Growth **186**, 214 (1998).
[50] P. G. Vekilov, J. I. D. Alexander, and F. Rosenberger (unpublished).